J. Fluid Mech. (1998), *vol.* 366, *pp.* 211–237. Printed in the United Kingdom

The evolution of a perturbed vortex in a pipe to axisymmetric vortex breakdown

By Z. RUSAK, S. WANG AND C. H. WHITING

Department of Mechanical Engineering, Aeronautical Engineering and Mechanics, Rensselaer Polytechnic Institute, Troy, NY 12180-3590, USA

(Received 10 June 1996 and in revised form 9 February 1998)

The evolution of a perturbed vortex in a pipe to axisymmetric vortex breakdown is studied through numerical computations. These unique simulations are guided by a recent rigorous theory on this subject presented by Wang & Rusak (1997*a*). Using the unsteady and axisymmetric Euler equations, the nonlinear dynamics of both small-and large-amplitude disturbances in a swirling flow are described and the transition to axisymmetric breakdown is demonstrated. The simulations clarify the relation between our linear stability analyses of swirling flows (Wang & Rusak 1996*a*, *b*) and the time-asymptotic behaviour of the flow as described by steady-state solutions of the problem presented in Wang & Rusak (1997*a*). The numerical calculations support the theoretical predictions and shed light on the mechanism leading to the breakdown process in swirling flows. It has also been demonstrated that the fundamental characteristics which lead to vortex instability and breakdown in high-Reynolds-number flows may be calculated from considerations of a single, reduced-order, nonlinear ordinary differential equation, representing a columnar flow problem. Necessary and sufficient criteria for the onset of vortex breakdown in a Burgers vortex are presented.

1. Introduction

The breakdown of vortex cores is a remarkable phenomenon in fluid dynamics which refers to the significant change in structure of high-Reynolds-number vortex flows with a high level of swirl. The breakdown phenomenon is characterized by the sudden appearance of a free stagnation point in the flow followed by large regions of flow reversal and increased turbulence levels. Experimental results of swirling flows in pipes exhibit several distinct forms of vortex breakdown. They range from weak helical disturbances to the stronger, spiral or nearly axisymmetric types (see, for example, Sarpkaya 1971; Leibovich 1978, 1984; Delery 1994; Bruecker & Althaus 1995; Sarpkaya 1995*b*). The various types of breakdown may develop in flows with the same Reynolds number, with only a small change in the swirl ratio (ratio of circumferential speed to axial speed) of the flow. This special behaviour of rotating flows is still considered a basic, largely unexplained phenomenon in modern fluid dynamics with a variety of technological applications and scientific interest.

Several review papers on this subject have been presented, including Hall (1972), Leibovich (1978, 1984), Escudier (1988), Delery (1994), Althaus, Bruecker & Weimer (1995) and Sarpkaya (1995*a*). These papers show that several possible explanations have been advanced, each clarifying some aspects of the problem. However, most of the previous efforts to explain vortex breakdown are based on local analyses and,

therefore, mask important information on the possible time evolution of swirling flows. Also, the relationship between the various theoretical and numerical solutions has never been fully clarified. Until recently, no clear global criteria for the occurrence, stability or dynamics of vortex breakdown states have been provided. The study in this paper is motivated by this complicated phenomenon.

A variety of numerical studies have been carried out over the last twenty five years to simulate the vortex breakdown phenomenon. Of specific interest to this paper are the investigations of axisymmetric vortex breakdown in a pipe using the axisymmetric Euler or Navier–Stokes equations. These works include Kopecky & Torrance (1973), Grabowski & Berger (1976), Krause (1985), Hafez & Salas (1985), Menne (1988), Salas & Kuruvila (1989) and Spall & Gatski (1991). These numerical studies demonstrated that axisymmetric vortex breakdown states may be successfully simulated and show some similarity with the physical situation and the experimental data.

In an effort to understand the complicated phenomenon of vortex breakdown, Beran & Culick (1992) constructed numerical solutions of a swirling flow in a pipe using the axisymmetric and steady Navier–Stokes equations. Numerical continuation methods were used in this work to derive the bifurcation diagram of solutions for fixed profiles of the axial and swirl velocity components entering the pipe as the swirl level of the incoming flow was changed. A schematic diagram of their results is given in figure 1 of Wang & Rusak (1997*a*). In this figure ω represents the level of swirl of the flow entering the pipe and $\min(w(x,0))$ is the minimum axial speed found on the vortex axis in a given solution. When the Reynolds number was sufficiently large, Beran & Culick (1992) found that there exist two limit points of the incoming swirl level, ω, which connect three distinct branches of steady-state solutions. Along the branch of solutions (*a*) ω increases up to the first limit point and this branch describes near-columnar flows along the pipe. The branch of solutions (*b*) starts from the first limit point and ends at the secondary limit point; along this branch the incoming swirl is reduced. Solutions along this fold describe a swirling flow with a localized standing wave that develops into a localized separation zone as the swirl approaches the secondary limit point. The branch of solutions (*c*) starts from the secondary limit point; along this branch the incoming swirl is increased and solutions describe a large separation zone in the swirling flow. Beran & Culick (1992) indicated that there may be a possible relation between the first limit point in their computations and the critical swirl, ω_B, defined by Benjamin (1962) (see figure 1 in Wang & Rusak 1997*a*).

Recently, Lopez (1994) and Beran (1994) studied the dynamics of swirling flows using the unsteady and axisymmetric Navier–Stokes equations. Both of these studies showed that the aforementioned branches of solutions (*a*) and (*c*) are stable to small, axisymmetric disturbances, whereas the solutions along branch (*b*) (in the fold) are unstable. Steady-state solutions along branch (*b*) cannot develop in a dynamical process starting from any initial swirling flow. Moreover, if a solution along the fold is given as the initial state, it will evolve in time into one of the other (stable) states along branches (*a*) or (*c*).

In an inviscid, steady-state approach, relevant to the present work, Keller, Egli & Exley (1985) described the axisymmetric vortex breakdown in an infinitely long straight pipe as an open stagnation zone of free boundaries that appears in the base vortex flow. Their solution describes a transition from a base, upstream, columnar state described by the Rankine vortex, to another, downstream, columnar state that has the same 'flow force' (resulting from the conservation of axial momentum along the pipe); both states are solutions of the same columnar problem. However, a careful understanding of this solution shows that when the vortical core radius of the base

(upstream) state is fixed, the solution is limited only to a specific value of the swirl ratio, defined later in this paper as ω_0, where $\omega_0 < \omega_B$. For this special solution $\min(w(x,0)) = 0$ (see figure 1 in Wang & Rusak 1997*a*).

The reviews of the theoretical and numerical studies on vortex stability and breakdown (see Leibovich 1978, 1984; Althaus *et al.* 1995; Ash & Khorrami 1995; Rusak & Wang 1996*a*) demonstrate that no previous analyses of swirling flows can provide clear insight into the special behaviour of the numerical solutions of Beran & Culick (1992), Beran (1994) and Lopez (1994). The relation between the critical swirl and the first limit point as suggested by Beran & Culick (1992) is not completely understood. Also, there is no explanation for the existence of the secondary limit point that appears in the viscous computations and its possible relation to the special solution of Keller *et al.* (1985). It should also be emphasized that none of the known stability analyses can shed any light on the specific stability characteristics of the solutions described by Beran (1994) and Lopez (1994).

Wang & Rusak (1997*a*) have recently presented a novel theoretical approach which describes the axisymmetric vortex breakdown process (see also Rusak & Wang 1996*a*, *b* and Wang & Rusak 1996*c*). This approach, employing the unsteady Euler formulation, examines the dynamics of axisymmetric swirling flows in a straight pipe of finite length. The analysis concentrates on studying the initial growth tendency of a perturbation in a swirling flow as it relates to the stability characteristics of the flow (see Wang & Rusak 1996*a*, *b*), as well as the relation of the time-asymptotic behaviour of the flow to the steady-state solutions. The results are established through a rigorous mathematical analysis and provide a fundamental, and nearly complete, theoretical understanding of the dynamics of axisymmetric swirling flows. The stability analyses together with the steady-state solutions suggest a consistent explanation of the mechanism leading to the axisymmetric vortex breakdown process in high-Reynolds-number flows. This process is the evolution from an initial columnar vortex flow to another relatively stable and lower-energy equilibrium state of a swirling flow around a large separation zone. This evolution is a result of the interaction between disturbances propagating upstream and the incoming flow to the pipe which leads to a loss of stability of the base columnar state when the swirl ratio of the incoming flow is near or above the critical level. The effect of slight viscosity as well as small pipe divergence on the flow dynamics and the transition to vortex breakdown has been recently studied by Wang & Rusak (1997*b*) and Rusak, Judd & Wang (1997).

The theoretical effort of Wang & Rusak (1997*a*) provides a framework in which computations of the vortex breakdown process can be conducted. We present in this paper numerical simulations of the axisymmetric and inviscid vortex breakdown in a pipe that are guided by this theory. The outline of the paper is as follows. A summary of the mathematical problem and the theoretical approach is given in § 2. The method of computing the bifurcation points and its application to the Burgers vortex model are discussed in § 3. Inviscid simulations of the axisymmetric vortex breakdown in a pipe are described in § 4. In § 5 we summarize the dynamics of an axisymmetric swirling flow in a pipe and provide necessary and sufficient criteria for the onset of breakdown in a Burgers vortex. It should be emphasized that the present numerical simulations use well-known finite difference techniques to solve the time-dependent flow problem and the major objective in this paper is to demonstrate the relation between the numerical simulations and the theoretical studies of Wang & Rusak (1996*a*, *b*, 1997*a*).

The present approach is limited to the axisymmetric and inviscid dynamics of swirling flows. This may be a problematic limitation of the theory since numerous

experimental and numerical results show the existence of helical instabilities in the wake of the axisymmetric bubble zone and, more specifically, in certain cases, the evolution of the nearly axisymmetric breakdown into a spiral type of breakdown (see, for example, the experimental works of Sarpkaya 1971; Leibovich 1984 and Bruecker & Althaus 1995 and the numerical studies of Tromp & Beran 1996, 1997; Spall 1996; Visbal 1996 and Cary, Darmofal & Powell 1997).

It can be shown, however, that according to normal-mode stability analyses, in the range of swirl of interest (near the critical swirl, ω_B of Benjamin 1962, or its correction for a finite length pipe given by Wang & Rusak 1997*a*, denoted as ω_1) the base columnar vortex flows are usually neutrally stable to both axisymmetric and three-dimensional infinitesimal disturbances. For example, the review paper of Leibovich (1984, figure 8) provides instability regions for the Q-vortex model and shows that for relevant vortex flows these are much below the critical swirl, ω_1. Also, inlet vortex flows to a pipe that later experienced breakdown are usually stable to both axisymmetric and three-dimensional small disturbances. Moreover, as we find in the present computations, these instability regions are even below the critical level, ω_0, for large-amplitude axisymmetric disturbances, described in Wang & Rusak (1997*a*). Therefore, we find that for relevant experimental vortex flows (such as those reported in Leibovich 1984) large-amplitude disturbances or the breakdown zones cannot evolve from an infinitesimal periodic disturbance on a columnar flow. It is only the specific inviscid axisymmetric instability mechanism, recently revealed by Wang & Rusak (1996*a*) which is related to a non-periodic mode of disturbance, that actually exists at the swirl levels of interest in such high-Reynolds-number flows. This special instability mechanism depends on the swirl separation from the critical swirl ω_1 and is demonstrated in the present computations and matches with our theoretical predictions.

Moreover, we use the unsteady simulations to follow the nonlinear dynamics of small- or large-amplitude disturbances and, specifically, the unstable axisymmetric disturbance as it evolves in time into the axisymmetric breakdown. We find that the time-asymptotic solutions resulting from the present simulations match with the steady-state solutions of the axisymmetric Euler equations described in Wang & Rusak (1997*a*). The current numerical calculations provide, in this way, the transient nonlinear dynamics linking our new stability results (Wang & Rusak 1996*a*, *b*) and our new steady-state results (Wang & Rusak 1997*a*). They help to clarify the appearance of the axisymmetric breakdown process as it is related to both issues. They also demonstrate the nature of the swirl level, ω_0 (of Keller *et al.* 1985), as a critical state for finite-amplitude axisymmetric disturbances, related to the secondary limit point found in the Navier–Stokes computations of Beran & Culick (1992).

The present numerical studies also help to identify the nature of the inviscid flow in the breakdown zone and the relevant continuation method to be used inside this zone in the study of steady-state solutions of the Euler equations. There may exist an infinite number of continuation methods in the steady and inviscid framework, but it is the flow dynamics of a perturbed columnar vortex state that actually clarifies the nature of the separation zone as a stagnation zone. It should be emphasized that this flow characteristic appears naturally, with no special assumptions with regard to the inviscid dynamics of the flow. It also matches with various experimental and numerical results on high-Reynolds-number vortex flows where it is shown that the flow is essentially stagnant in the breakdown zone (see, for example, Escudier 1988; Lopez 1994). In this way the present numerical simulations help to complete the relationship between our stability and steady-state analyses of swirling flows and

provides a nearly complete description of solutions of the axisymmetric and inviscid problem.

Finally, we comment on the importance of the axisymmetric analysis even in flow situations where large three-dimensional disturbances dominate the flow. The experimental results of Sarpkaya (1971), Bruecker & Althaus (1995), and Althaus *et al.* (1995) demonstrate the existence of certain swirling flows with nearly axisymmetric and inviscid dynamics leading to the appearance of axisymmetric breakdown zones. It is only after the axisymmetric breakdown zone is more or less established in the swirling flow, that three-dimensional disturbances appear inside the breakdown zone and its wake. Those disturbances may even become unstable under certain conditions and grow to finite-amplitude disturbances and unsteady three-dimensional vortical flows may develop and never settle to a steady state. In some situations the nearly axisymmetric breakdown state may evolve to a spiral breakdown state as was found in the experiments of Bruecker & Althaus (1995). Similar behaviour has recently been described in the numerical simulations using the unsteady Navier–Stokes equations by Tromp & Beran (1996, 1997), Spall (1996), Visbal (1996) and Cary *et al.* (1997).

According to our understanding, the three-dimensional disturbances that develop in the aforementioned flows should be viewed as symmetry-breaking instabilities from the axisymmetric breakdown states found from our theory, and not from the base columnar vortex flow. As is already pointed out above, stability analyses show that in the range of swirl of interest, the base columnar vortex state is usually neutrally stable to three-dimensional infinitesimal disturbances. Therefore, we may conclude that there exist relevant swirling flow situations where, for a long time or for some time period, the transient dynamics is dominated by an axisymmetric and inviscid behaviour. In some of the situations, the transition from a concentrated vortex to the axisymmetric breakdown state is a crucial step in the evolution of non-axisymmetric breakdown states. This point of view clarifies the important role of the mechanism leading to axisymmetric breakdown studied in this paper, even in situations where at the end a large-amplitude, non-axisymmetric unsteady disturbance appears in the flow. We believe that in order to explore the dynamics of three-dimensional swirling flows it would appear important to extend our theoretical framework to investigate the evolution of three-dimensional disturbances from columnar states as well as from the axisymmetric breakdown states found in our study.

2. Theoretical approach

2.1. *Mathematical model*

An unsteady, axisymmetric, incompressible and inviscid flow with swirl has been considered in a finite length pipe of unit radius, the centreline of which is the x-axis and where $0 \leqslant x \leqslant x_0$. The axial and radial distances are rescaled with the radius of the pipe, r_t. By virtue of the axisymmetry, a stream function $\psi(x, r, t)$ can be defined where the radial component of velocity $u = -\psi_x/r$, and the axial component of velocity $w = \psi_r/r$. Let $y = r^2/2$, then the azimuthal vorticity η is given by $\eta = r\chi$ where $\chi = -(\psi_{yy} + \psi_{xx}/2y)$. The circulation function K is defined as $K = rv$ where v is the circumferential velocity component. The equations which connect the development in time (t) of the stream function ψ, the function χ and the circulation function K may be given by (see, for example, Szeri & Holmes 1988)

$$K_t + \{\psi, K\} = 0, \quad \chi_t + \{\psi, \chi\} = \frac{1}{4y^2}(K^2)_x \quad \text{on} \quad 0 \leqslant x \leqslant x_0, \quad 0 \leqslant y \leqslant 1/2. \qquad (1)$$

Here the brackets $\{\psi, K\}$ and $\{\psi, \chi\}$ are defined by

$$\{\psi, K\} = \psi_y K_x - \psi_x K_y, \quad \{\psi, \chi\} = \psi_y \chi_x - \psi_x \chi_y. \tag{2}$$

We study the development of the flow with certain conditions posed on the boundaries. For all time, t, we set $\psi(x, 0, t) = 0$ to satisfy the axisymmetric condition along the pipe centreline, $y = 0$, and $\psi(x, 1/2, t) = \overline{w}_0$ along the pipe wall, $y = 1/2$, to describe the total mass flux across the pipe. Also, for all time, the incoming flow along the pipe inlet is given by the axial flow and circulation as

$$\psi(0, y, t) = \psi_0(y), \; K(0, y, t) = \omega K_0(y). \tag{3}$$

Here ω reflects the swirl level of the incoming flow. We also consider the case where $\psi_{xx}(0, y, t) = 0$ to fix the azimuthal vorticity along the inlet at any time t,

$$\chi(0, y, t) = -\psi_{0yy}. \tag{4}$$

We allow the inlet state a certain degree of freedom to develop a radial velocity, to reflect the upstream influence of disturbances that have the tendency to manifest themselves as instabilities. The boundary conditions along the pipe outlet section depend on the physical situation. However, boundary conditions that result in a well posed mathematical problem may relate to certain physical situations of interest. The method given in this paper is general and can handle various conditions, but in order to demonstrate our idea we concentrate on specific outlet conditions. To this end, we specify only one condition along the pipe outlet. We assume no radial speed along $x = x_0$, i.e.

$$\psi_x(x_0, y, t) = 0. \tag{5}$$

Similar boundary conditions have been considered by Salas & Kuruvila (1989), Beran & Culick (1992), Beran (1994), Lopez (1994) and Tromp & Beran (1996, 1997) in their numerical simulations using the Navier–Stokes equations and by Buntine & Saffman (1995) in their theoretical study of steady swirling flows in a finite-length diverging pipe using the Euler equations. They may also reflect the physical situation as reported in the experiments of Bruecker & Althaus (1995).

The problem defined by equations (1)–(5) is well posed and describes the evolution of a swirling flow in a finite-length pipe. It is strongly expected that starting from some relevant initial conditions for the stream function, circulation and azimuthal vorticity, such as a columnar state along the pipe, i.e.

$$\psi(x, y, 0) = \psi_0(y), \quad K(x, y, 0) = \omega K_0(y), \quad \chi(x, y, 0) = -\psi_{0yy} \tag{6}$$

the flow will develop uniquely in time after a disturbance is introduced to the flow. Drazin & Howard (1965) proved uniqueness of a time-dependent solution of the Euler equations for similar boundary conditions and any initial state. Moreover, we will show that the axisymmetric vortex breakdown is primarily related to the swirl level, ω, of the incoming flow.

2.2. *Summary of the theoretical study*

The theory is composed of two major steps:

(*a*) Global variational analysis of steady-state solutions of the axisymmetric Euler equations (1) (resulting in the Squire–Long equation). In this analysis, a functional, $\mathscr{E}(\psi)$ (see details later in equation (10)), whose stationary points correspond to solutions of the Squire-Long equation, was studied in detail. This variational principle was first introduced into the study of vortex breakdown by Benjamin (1962) and was

also used by Keller *et al.* (1985). For more details of this approach see Wang & Rusak (1997*a*) and specifically figures 13 and 15 therein.

(*b*) Linear stability analysis of these various steady-state solutions (see Wang & Rusak 1996*a*, *b*).

The theory shows the following.

(i) As the swirl level of the incoming flow is increased, there exist two bifurcation points $\omega_0 + \epsilon(x_0)$ and ω_1. Here, $\omega_0 < \omega_1$ and $\epsilon(x_0)$ is a small number that reflects the effect of the pipe length, and tends to zero as x_0 tends to infinity (see figure 13 in Wang & Rusak 1997*a*). ω_1 is the critical swirl for a flow in a finite pipe. When the pipe length is increased, ω_1 approaches Benjamin's (1962) critical swirl ω_B. The details of the methods of computing ω_0 and ω_1 and the physical meaning of these special swirl levels are given in §3.

(i)(*a*) When $\omega < \omega_0$, only a columnar flow solution exists, which is the global minimizer of $\mathscr{E}$. ω_0 is a bifurcation point where a breakdown solution may develop for the first time. When $\omega > \omega_0 + \epsilon(x_0)$ three solutions exist. One is a columnar flow solution which now becomes a local minimizer of $\mathscr{E}$. Two other solutions, a global minimizer and a min-max solution, bifurcate at ω_0, and both describe vortex breakdown solutions. It can be shown that the min-max solution describes a swirling flow with a localized wave similar to the solitary wave solution of Leibovich & Kribus (1990). The global minimizer solution describes a swirling flow around an open stagnation zone which is a transition along the pipe axis from the given inlet state to a certain outlet state. The outlet state is a global minimizer solution of the ODE resulting from the Squire–Long equation for the columnar (x-independent) problem.

(i)(*b*) As $\omega \to \omega_1^-$, the branch of min–max solutions approaches the branch of columnar flows and ω_1 is a transcritical bifurcation point. When $\omega > \omega_1$ the columnar flows become min-max solutions and another branch of local minimizer, non-columnar, flow solutions bifurcates at ω_1 (see figure 13 in Wang & Rusak 1997*a*).

(ii) Linear stability analysis of axisymmetric disturbances using (1)–(5) shows (see figure 15 in Wang & Rusak 1997*a*) that the critical swirl level, ω_1, is also a point of exchange of stability; the branches of local minimizers of $\mathscr{E}$ bifurcating at ω_1 have an asymptotically stable mode of disturbance whereas the min-max solutions are unstable. Specifically, an unknown mechanism of instability has been revealed by Wang & Rusak (1996*a*) for the branch of columnar swirling flows in a finite length pipe. This instability mechanism relates the upstream propagation of disturbances along the vortex core and the nature of the inlet flow. It has been shown that the disturbances are convected out of the pipe and columnar rotating flows are linearly stable when $\omega < \omega_1$. However, the disturbances tend to move upstream, interact with the inlet flow, grow and destabilize the columnar state when $\omega > \omega_1$. Such a mechanism cannot be predicted by any of the previously known stability analyses of swirling flows and is crucial to the understanding of the axisymmetric vortex breakdown phenomenon which will be demonstrated in our numerical simulations described in §4.

(iii) These results suggest an explanation for the physical mechanism leading to the axisymmetric vortex breakdown phenomenon in a swirling flow in a finite length pipe: it is a transition phenomenon, that may occur only when $\omega > \omega_0 + \epsilon(x_0)$, from a columnar vortex flow, that loses its stability margin as ω tends ω_1, into another steady and stable global minimizer solution that is a strong attractor. When $\omega > \omega_1$, any perturbation will induce this transition. The swirl level ω_0 is a threshold level for a steady and stable axisymmetric breakdown and the condition $\omega > \omega_0$ is a necessary

condition for breakdown to appear. The condition $\omega > \omega_1$ is a sufficient condition for breakdown.

The theory provides for the first time a consistent explanation of the physical mechanism leading to the axisymmetric vortex breakdown phenomenon in a pipe as well as the conditions for its occurrence. Also, as demonstrated in Rusak & Wang (1996*a*, *b*), the theory that is based on the analysis of solutions of the time-dependent problem (1)–(6), unifies previous theoretical approaches to vortex breakdown, fills the void between those approaches, constructs the relationship between stability to axisymmetric disturbances and criticality of swirling flows and sheds light on the numerical simulations of this phenomenon (Rusak & Wang 1996*a*). For the detailed mathematical analysis of the phenomenon see Wang & Rusak (1997*a*, 1996*a*, *b*).

In this paper we first demonstrate the methods to calculate the bifurcation points ω_0 and ω_1 of the steady-state problem resulting from (1)–(6) where the inlet state is described by the Burgers vortex model:

$$\psi_0(y) = y, \quad \omega K_0(y) = \omega(1 - \mathrm{e}^{-2\beta y}). \tag{7}$$

Here ω is the swirl level and β is related to the size of the vortical core, $r_c/r_t = 1.12/\beta^{1/2}$. It is shown that $\omega_0(\beta)$ can be calculated from solutions of the ODE resulting from the x-independent Squire–Long equation, and that $\omega_1(\beta)$ can be calculated from the linearized ODE. Subsequently, we demonstrate by numerical simulations based on equations (1)–(7) the relation between stability and criticality of a columnar vortex flow in a finite-length pipe and provide insight into the dynamical process of the transition from columnar flow states to breakdown states. These breakdown states correspond to the previously discussed global minimizer solutions predicted by the theory. Results are summarized in terms of basic criteria for the development of axisymmetric vortex breakdown in a swirling flow given by the Burgers vortex model.

3. Calculation of ω_0 and ω_1 for a Burgers vortex

Wang & Rusak (1997*a*) analysed solutions of the Squire–Long equation (SLE) (resulting from (1) for a steady-state case and also known as the Bragg–Hawthorne 1950 equation)

$$\psi_{yy} + \psi_{xx}/2y = H'(\psi) - I'(\psi)/2y \quad \text{on} \quad 0 \leqslant x \leqslant x_0, \quad 0 \leqslant y \leqslant 1/2, \tag{8}$$

with boundary conditions

$$\left.\begin{aligned} \psi(x,0) = 0, \quad \psi(x,1/2) = 1/2, \\ \psi(0,y) = \psi_0(y), \quad K(0,y) = \omega K_0(y), \quad \psi_x(x_0,y) = 0 \end{aligned}\right\} \tag{9}$$

that describe the development of a steady flow in a pipe of length x_0. Here, $H = p/\rho + (u^2 + w^2 + v^2)/2$ is the total head function, and $I = (rv)^2/2$ is the extended circulation, both of which are functions of ψ only. For more details on (8) see Batchelor (1967).

Solutions of the SLE are well-known to correspond to the stationary points of the following functional, $\mathscr{E}(\psi)$, (see also Keller *et al.* 1985)

$$\mathscr{E}(\psi) = \int_0^{x_0} \int_0^{1/2} \left(\frac{\psi_y^2}{2} + \frac{\psi_x^2}{4y} + H(\psi) - \frac{I(\psi)}{2y} \right) \mathrm{d}y \, \mathrm{d}x. \tag{10}$$

It has been found that the variational functional $\mathscr{E}(\psi)$ has a complicated behaviour as the incoming swirl ω is varied. Through a careful estimation of the various integrals

in (10) Wang & Rusak (1997*a*) proved the existence of the global minimizer $\psi_g(x, y)$ of $\mathscr{E}(\psi)$ when both $H(\psi)$ and $I(\psi)$ are bounded, reflecting the boundedness of energy and circulation in the pipe. Wang & Rusak (1997*a*) have also shown that the global minimizer solution $\psi_g(x, y)$ is dominated by the global minimizer solution $\psi_s(y)$ of the columnar problem (where $\psi_x = \psi_{xx} = 0$)

$$\psi_{yy} = H'(\psi) - I'(\psi)/2y, \quad \psi(0) = 0, \quad \psi(1/2) = 1/2 \tag{11}$$

with the corresponding variational functional

$$E(\psi) = \int_0^{1/2} \left(\frac{\psi_y^2}{2} + H(\psi) - \frac{I(\psi)}{2y} \right) \mathrm{d}y. \tag{12}$$

For a solution of (11) this functional represents the flow force as defined by Benjamin (1962). Wang & Rusak (1997*a*) have found that there exists a certain swirl level, ω_0, such that when $\omega < \omega_0$ the global minimizer solution of the ODE (11) is $\psi_s(y) = \psi_0(y)$, which implies that the global minimizer solution of the PDE (8) is the columnar flow $\psi_g(x, y) = \psi_0(y)$. However, when $\omega > \omega_0$ the global minimizer solution $\psi_s(y)$ of the ODE (11) is quite different than $\psi_0(y)$, with $E(\psi_s(y)) < E(\psi_0(y))$, and contains a separation region in the domain $0 \leqslant y \leqslant y_a$. Therefore, the global minimizer of the PDE (8) describes a non-columnar vortex breakdown solution along the pipe which is a transition from an inlet state $\psi_g(0, y) = \psi_0(y)$ to an outlet state $\psi_g(x_0, y) = \psi_s(y)$ and where the difference $E(\psi_0(y)) - E(\psi_s(y)) = \int_0^{1/2} \psi_x^2(0, y)/2y \, \mathrm{d}y$ creates a radial flow along the pipe inlet. At the swirl level ω_0 we have $E(\psi_s(y)) = E(\psi_0(y))$. It should be noted that Keller *et al.* (1985) used a similar technique to compute their special vortex breakdown solutions for an inlet state described by the Rankine vortex. However, for a fixed vortical core radius, their solutions are limited only to the swirl level defined in this paper as ω_0.

It should also be noticed that the global minimizer of $E(\psi)$ depends on the choice of a continuation model in the separation zone. Different choices will result in different global minimizer solutions of the ODE. However, since we look for the solution of the ODE (11) which represents the outlet state of the global minimizer solution of the PDE (8), we have to choose a continuation model that is relevant to the solution of the dynamical problem given by (1)–(6). It is expected that solutions of (1)–(5) with initial conditions (6) will evolve with no reversed flow along the outlet or inside the domain. The numerical simulations based on (1)–(6) described in §4 support this idea and clearly show the establishment of a stagnation zone when $\omega > \omega_0$ as time tends to infinity. Regions of essentially stagnant flow have also been found in the numerical simulations of Lopez (1994) based on the Navier–Stokes equations. It, therefore, seems plausible to choose a stagnation model in the search for the global minimizers of both the PDE (8) and the ODE (11). A similar choice was made by Keller *et al.* (1985) in their special inviscid vortex breakdown solutions.

In the case of the Burgers vortex model (7), the following relations are found,

$$I'(\psi) = 2\beta\omega^2(1 - \mathrm{e}^{-2\beta\psi})\mathrm{e}^{-2\beta\psi}, \quad H'(\psi) = I'(\psi)/2\psi$$

and (11) becomes

$$\psi_{yy} = \beta\omega^2(1 - \mathrm{e}^{-2\beta\psi})\mathrm{e}^{-2\beta\psi}(1/\psi - 1/y), \quad \psi(0) = 0, \quad \psi(1/2) = 1/2. \tag{13}$$

It can be shown that solutions of (13) and their first derivatives are continuous. For fixed values of β and ω we numerically integrate (13) using a standard Runge–Kutta integration scheme of *Mathematica*. We look for solutions of (13) where,

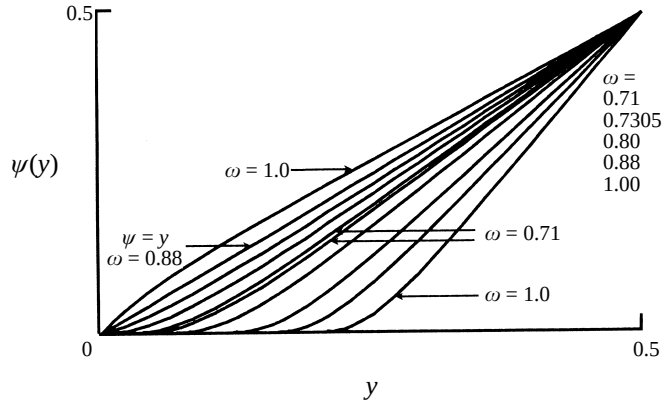

FIGURE 1. Solutions of (13) for a Burgers' vortex model with $\beta = 4.0$.

specifically, $0 \leqslant \psi \leqslant 1/2$ in the domain $0 \leqslant y \leqslant 1/2$ and where a stagnation region with $\psi = 0$ may appear in the solution in a finite region $0 \leqslant y \leqslant y_a$ and where $\psi(y_a) = \psi_y(y_a) = 0$. Equation (13) together with these conditions at $y = y_a$ completely specify a free boundary value problem from which the size of the stagnation zone, y_a, may be determined as a function of the swirl level. Details of the computational methods to solve this problem are given in Whiting (1996). It is important to notice that there exist other solutions of (13) with reversed flow regions where $\psi < 0$ in a certain region of the domain $(0, 1/2)$ once another continuation model is used. However, those solutions are not relevant to the steady-state solutions found from the time-dependent and inviscid flow problem described by (1)–(6).

The solutions of (13) for various values of ω are presented in figure 1 for $\beta = 4.0$. Computations for other values of β show similar results (see Whiting 1996). We want to emphasize that these new, non-trivial solutions of the SLE (11) are of great interest since they contain information that helps to clarify the breakdown solutions of the PDE (8). We find that, in addition to the base solution $\psi = y$, there exist two other types of solutions that meet the above requirements: type I, where $\psi(0) = 0$ but $\psi_y(0) > 0$ and type II, where $\psi = 0$ in the domain $0 \leqslant y \leqslant y_a$ (stagnation region) and $\psi_y(y_a) = 0$. We also find that there exists a certain level of swirl $\omega^*(\beta)$ where for $\omega < \omega^*(\beta)$ only the base solution exists. The swirl level $\omega^*(\beta)$ is a bifurcation point of solutions of (13). At $\omega = \omega^*(\beta)$ we find two solutions: one is the base solution and the other is a special solution of type II. For example, when $\beta = 4.0$ we have $\omega^* = 0.7084\ldots$. When ω is slightly greater than $\omega^*(\beta)$ three solutions are found: one is the base solution and the other two, $\psi_1(y;\omega)$ and $\psi_2(y;\omega)$ have large and small stagnation regions, respectively. When ω is further increased the branch of $\psi_1(y;\omega)$ solutions of type II describes larger stagnation zones whereas the branch of $\psi_2(y;\omega)$ solutions with the small stagnation zone changes naturally into solutions of type I. The latter branch approaches the base solution as ω approaches the certain critical bifurcation point, ω_B, defined by Benjamin (1962). The critical level of swirl is the first eigenvalue of the linearized problem resulting from (13),

$$\phi_{yy} - \left(\frac{\psi_{0yyy}}{\psi_{0y}} - \omega^2 \frac{K_0 K_{0y}}{2y^2 \psi_{0y}^2} \right) \phi = 0, \quad \phi(0) = 0, \quad \phi(1/2) = 0. \tag{14}$$

This problem can also be solved numerically for any β using a standard eigenvalue solver based on a central difference approximation of the derivatives. For the case

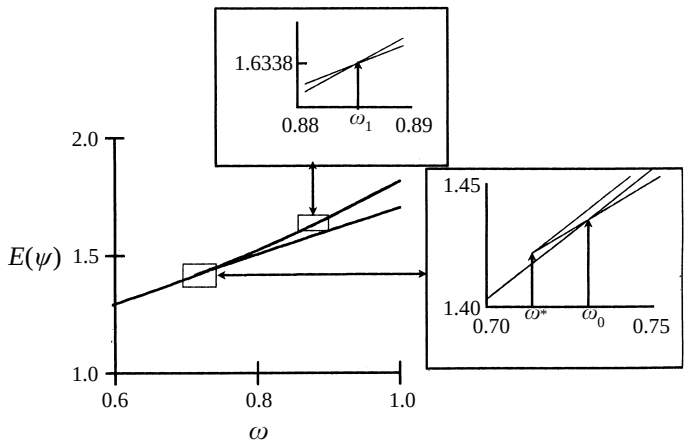

FIGURE 2. Bifurcation diagram of solutions of (13) for a Burgers vortex model with $\beta = 4.0$.

where $\beta = 4.0$ we find $\omega_B = 0.8829\ldots$. As ω is increased above ω_B a new branch of solutions of type I bifurcates at ω_B for which $\psi_{0y}(0) > 1$ (see figure 1).

According to the theory of Wang & Rusak (1997*a*), for each one of the solutions of the ODE (13), we calculate the flow force as given by (12) (see Whiting 1996 for more details of these computations). Results are shown in the bifurcation diagram in figure 2 for the case $\beta = 4.0$. Similar bifurcation diagrams can be constructed for any value of β. It can be seen that there exists a certain level of swirl defined as ω_0 for which $E(\psi_1) = E(\psi_0)$. For the case $\beta = 4.0$ we find that $\omega_0 = 0.7305\ldots$.

When $\omega^* < \omega < \omega_0$ we find $E(\psi_2) > E(\psi_1) > E(\psi_0)$ whereas for $\omega_0 < \omega < \omega_B$ we find $E(\psi_2) > E(\psi_0) > E(\psi_1)$. Following Wang & Rusak (1997*a*) we can conclude that $\psi_0(y)$ is a global minimizer of $E(\psi)$ when $\omega < \omega_0$ whereas $\psi_1(y;\omega)$ is a global minimizer of $E(\psi)$ when $\omega > \omega_0$. It can also be shown that in the region $\omega_0 < \omega < \omega_B$, the solution $\psi_2(y;\omega)$ is a min-max point of $E(\psi)$. When $\omega > \omega_B$, we have $E(\psi_0) > E(\psi_2) > E(\psi_1)$ which implies that in this range the base solution, ψ_0, is a min-max point and the solution ψ_2 is a local minimizer of $E(\psi)$.

These results show similar behaviour to the theoretical discussion on the Rankine vortex model described in Wang & Rusak (1997*a*).

A further discussion of the critical level of swirl is now appropriate. For a swirling flow in a pipe of length x_0, the critical swirl, ω_1, is computed according to Wang & Rusak (1997*a*) as the first eigenvalue of the linearized problem of (8), i.e.

$$\phi_{yy} - \left(\frac{\pi^2}{8x_0^2 y} + \frac{\psi_{0yyy}}{\psi_{0y}} - \omega^2 \frac{K_0 K_{0y}}{2y^2 \psi_{0y}^2} \right) \phi = 0, \quad \phi(0) = 0, \quad \phi(1/2) = 0. \tag{15}$$

The problem (15), which is similar to (14), can be solved numerically for any value of β and x_0 using the same technique as above. For example, in the case when $\beta = 4.0$ and $x_0 = 6.0$ (to be discussed in §4) we find $\omega_1 = 0.8845\ldots$, which is very close to $\omega_B = 0.8829\ldots$. This demonstrates that ω_1 tends to Benjamin's critical swirl level, ω_B, as the length of the pipe is increased.

The bifurcation diagram in figure 2 can now be used to describe the steady-state solutions of the SLE (8)–(9). When $\omega < \omega_0$ only one steady-state solution will develop which describes a columnar flow. When $\omega_0 + \epsilon(x_0) < \omega < \omega_1$ we may find three steady-state solutions: one describes a columnar flow and is a local minimizer

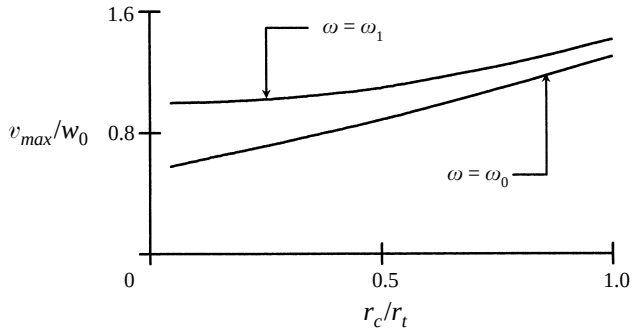

FIGURE 3. ω_0 and ω_1 as function of vortex core radius, $r_c/r_t = 1.12/\beta^{1/2}$.

of $\mathscr{E}(\psi)$; the second describes a swirling flow with a localized stagnation zone that disappears as ω is increased toward ω_1, and is a min-max point of $\mathscr{E}(\psi)$; the third describes a swirling flow around a stagnation zone and is the global minimizer of $\mathscr{E}(\psi)$. The size of the stagnation region in the last solution corresponds to that of the separation zone, y_a, of the ODE solution $\psi_1(y;\omega)$ and increases as ω is increased.

We can now conclude, through considerations of the stability analyses of Wang & Rusak (1996*a*, *b*), that only the local and global minimizer solutions are linearly stable to axisymmetric disturbances whereas the min-max solutions are unstable. Therefore, with regard to solutions of the dynamical problem defined by (1)–(6) we find that when $\omega < \omega_0$, only one steady-state solution, which is a columnar swirling flow, can develop. When $\omega_0 < \omega < \omega_1$, two steady-state solutions may develop depending on the initial disturbances to the base flow as given by (6). When $\omega > \omega_1$ we find that the time-dependent solution of (1)–(6) will always develop into the steady breakdown state described by the global minimizer solution of (8). We can infer that steady breakdown solutions can be found only when $\omega > \omega_0$ and when $\omega > \omega_1$ such breakdown solutions will always develop. The values of the swirl ratio v_{max}/w_0 for the Burgers vortex model (where $v_{max} = \omega\beta^{1/2}(1 - \exp(-1.12^2))/1.12$ and $w_0 = \psi_{0y} = 1$), that correspond to ω_0 and ω_1, as function of the vortex core radius over the pipe radius, $r_c/r_t = 1.12/\beta^{1/2}$, are presented in figure 3. This figure provides guiding criteria for the appearance of axisymmetric breakdown in a Burgers vortex coming into a pipe and is used in the following computations.

The simulations in the next section are guided by the theoretical results and demonstrate the expected behaviour of time-dependent solutions of (1)–(6) for various swirl levels of the incoming flow.

4. Inviscid simulations of axisymmetric vortex breakdown in a pipe

In this section we present numerical simulations of the time-dependent problem described by (1)–(6) where the inlet swirling flow is given by the Burgers vortex model (7). Since this problem is dominated by the propagation of disturbances in the axial direction (both downstream and upstream depending on the swirl level) we choose a suitable finite-difference scheme based on the Lax method. To accomplish this, a uniform mesh is employed for the spatial domain ($0 \leqslant x \leqslant x_0, 0 \leqslant y \leqslant \frac{1}{2}$) and the resulting discretized equations are

$$K_{i,j}^{n+1} = 0.5(K_{i+1,j}^{n} + K_{i-1,j}^{n}) - d[(\psi_{i,j+1}^{n} - \psi_{i,j-1}^{n})(K_{i+1,j}^{n} - K_{i-1,j}^{n}) - (\psi_{i+1,j}^{n} - \psi_{i-1,j}^{n})(K_{i,j+1}^{n} - K_{i,j-1}^{n})], \quad (16)$$

$$\chi_{i,j}^{n+1} = 0.5(\chi_{i+1,j}^{n} + \chi_{i-1,j}^{n}) - d[(\psi_{i,j+1}^{n} - \psi_{i,j-1}^{n})(\chi_{i+1,j}^{n} - \chi_{i-1,j}^{n}) - (\psi_{i+1,j}^{n} - \psi_{i-1,j}^{n})(\chi_{i,j+1}^{n} - \chi_{i,j-1}^{n})] + e[(K_{i+1,j}^{n})^2 - (K_{i-1,j}^{n})^2]/y_{i,j}^2. \quad (17)$$

Here, (i, j) labels a mesh point, n the time level, Δx is the axial step size, Δy is the transverse step size, Δt is the time step, $d = \Delta t/(4\Delta x \Delta y)$ and $e = \Delta t/(8\Delta x)$. The time step has been chosen such that the Courant number $C = \Delta t/\Delta x < 1.0$ to ensure that the scheme is numerically stable. At each time level, an iterative point relaxation algorithm based on a central-difference scheme has been implemented to solve the Poisson equation, $\psi_{yy} + \psi_{xx}/2y = -\chi$, for the stream function ψ. For an iteration number k we use

$$(\psi_{i,j}^{n})^{k+1} = (\psi_{i,j}^{n})^{k} - \frac{(G_{i,j}^{n})^{k}}{(\partial G_{i,j}^{n}/\partial \psi_{i,j}^{n})^{k}},$$

where

$$G_{i,j}^{n} = \frac{1}{(\Delta y)^2}(\psi_{i,j+1}^{n} - 2.0\psi_{i,j}^{n} + \psi_{i,j-1}^{n}) + \frac{1}{2y_{i,j}(\Delta x)^2}(\psi_{i+1,j}^{n} - 2.0\psi_{i,j}^{n} + \psi_{i-1,j}^{n}) + \chi_{i,j}^{n}$$

and $\partial G_{i,j}^{n}/\partial \psi_{i,j}^{n}$ is computed from $G_{i,j}^{n}$. The level of accuracy of solving the Poisson equation is measured by $\max_{i,j} |(G_{i,j}^{n})^{k}| < \tau = 10^{-5}$ for each time level n, which for the Δx and Δy used here results in $\max_{i,j} |(\psi_{i,j}^{n})^{k+1} - (\psi_{i,j}^{n})^{k}| < 10^{-8}$ for each time level n. It is found that changing τ to lower values only increases the number of iterations but does not affect the numerical solution of the flow dynamics. The entire numerical method is explicit, first order in time and second order in space. Starting from an initial state which is a perturbed columnar flow given by

$$\left.\begin{aligned} \psi(x, y, 0) &= \psi_0(y) + \delta \sin\left(\frac{\pi x}{2x_0}\right) \sin(2\pi y), \\ \chi(x, y, 0) &= -\psi_{0yy} + \delta A(y) \sin\left(\frac{\pi x}{2x_0}\right) \sin(2\pi y), \\ K(x, y, 0) &= K_0(y) + \frac{\delta K_{0y}}{\psi_{0y}} \sin\left(\frac{\pi x}{2x_0}\right) \sin(2\pi y), \end{aligned}\right\} \quad (18)$$

where $A(y) = (2\pi)^2 + (\pi/2x_0)^2/(2y)$, we use the above numerical scheme to integrate the solution in time and space.

We investigated the sensitivity of the numerical solutions to grid refinement and time step reduction. We concentrated on a Burgers vortex with $\beta = 4.0$ in a domain of length $x_0 = 6.0$. Two special test cases where $\omega = 0.7, \delta = -0.1$ and $\omega = 1.0, \delta = -0.1$ were investigated. Detailed discussions on these cases are given later in this section. In the first case, the flow is initially perturbed near the pipe centreline and the disturbance decays in time (see figure 4*a*), whereas in the second case the disturbance evolves into a breakdown solution (see below figure 8). Uniform meshes of 200 by 30 points and 400 by 60 points in the x- and y-directions, respectively, were used in the grid refinement analysis. Similar mesh step sizes were also used by Beran & Culick (1992), Beran (1994), Lopez (1994) and Tromp & Beran (1996, 1997) in their Navier–Stokes simulations of high-Reynolds-number flows and showed solutions insensitive to grid refinement. We find that a uniform mesh of 200 by 30 points provides sufficient accuracy for steady-state computations when compared with steady-state computations using more refined meshes of 400 by 60 points. The maximum absolute value of the variation of ψ and K at points in the flow field is no more than about

3%. It should be pointed out, however, that in the cases where large separation zones appear, variations of about 10% were found in the scaled azimuthal vorticity field, χ. Similar sensitivities of the numerical calculations was found in the simulations of Lopez (1994). It should also be emphasized here that a good correlation is found between the decay rate of a small disturbance when $\omega < \omega_1$ and the theoretical prediction of Wang & Rusak (1996*a*) (see figure 5). Moreover, the time-asymptotic states of the present simulations always show a good correlation of the downstream outlet flow with the outlet state predicted by the theoretical approach described above (see an example in figure 7). These points provide great confidence in the present calculations.

A Courant number, $C = 0.66$, was used in all of the computations. Numerical results for the above-mentioned test cases showed nice correlation with a case where the time step was reduced by one half. On the other hand, when C is increased to around 1.0 we find numerical instability problems. Our experience shows that the value $C = 0.66$ is found to be around an optimal value for efficient computations. The length of the pipe has also been varied and the steady-state results are quite similar for any $x_0 > 3.0$. It should be clarified, however, that, according to our theory, increasing the pipe length to infinity should result in convergence of the outlet flow profile to the theoretically predicted columnar state found as a solution of (11).

Several values of ω have been considered with $\beta = 4.0$ and $x_0 = 6.0$. Other cases can be studied in the same way. To illustrate the nature of the solutions found, time-history streamline contours of $\psi(x, y, t)$ for various values of ω and δ are presented in figures 4(*a*), 4(*b*), 6(*a*) and 8–11. In each frame in these figures, the lower streamline represents the pipe centreline (also the x-axis) and along this line $\psi = 0$, the upper streamline represents the pipe wall and along this line $\psi = 0.5$, the vertical axis is the y-axis, the flow runs from left to right and lines of constant ψ (with values $\psi = 0.0$, 0.001, 0.012, 0.025, 0.05, 0.10, 0.15, 0.20, 0.25, 0.30, 0.35, 0.40, 0.45, 0.5) are presented.

(i) $\omega = 0.7$: in this case $\omega < \omega_0 = 0.7305$ and the base columnar flow is unconditionally stable to any axisymmetric disturbance. Starting with an initial state (18) with $\delta = -0.1$ we can see (figure 4*a*) that the disturbance is convected downstream for all time, where some nonlinear effects are evident from the change of the shape of the wave in time. After about 38.0 time units, r_t/w_0 (where r_t is the pipe radius and $w_0 = \psi_{0y}$), the flow returns to a columnar state and stays there as expected. To demonstrate the unconditional stability of the base columnar flow we also investigate the case where the initial disturbance is much larger, $\delta = -0.2$, and includes a reversed flow region (see figure 4*b*). We find that even the larger disturbance is relatively quickly convected downstream out of the computational domain and, again, the flow returns to a steady columnar state after about 57.0 time units.

The convergence to a columnar state in these cases is also demonstrated by the time-history plots of a norm of the difference of the temporal solution from the columnar state, defined as $\Delta_\psi^n = \max_{i,j}(|\psi_{i,j}^n - \psi_{0j}|)$ (see figure 5). Here, $\psi_{0j} = \psi_0(y_j)$. It can be seen that in the two cases for $\omega = 0.7$ the dynamics of the disturbance is similar: after a nonlinear transient and when the perturbation becomes sufficiently small, Δ_ψ^n decays exponentially, $\Delta_\psi^n \sim \exp(-\sigma t)$, and with almost the same rate of decay σ. This behaviour is predicted by the stability analysis of Wang & Rusak (1996*a*). For $\beta = 4.0, x_0 = 6.0$ and swirl level $\omega = 0.7$ we find $\sigma \sim -0.208 w_0/r_t$.

(ii) $\omega = 0.8$: in this case $\omega_0 = 0.7305 < \omega < \omega_1 = 0.8845$ (here we used (15) to compute ω_1) and the flow may develop into one of two possible steady-state solutions, depending on the size of the initial disturbances. When $\delta = -0.02$ (a relatively small disturbance) the disturbance is convected downstream as the linear stability theory

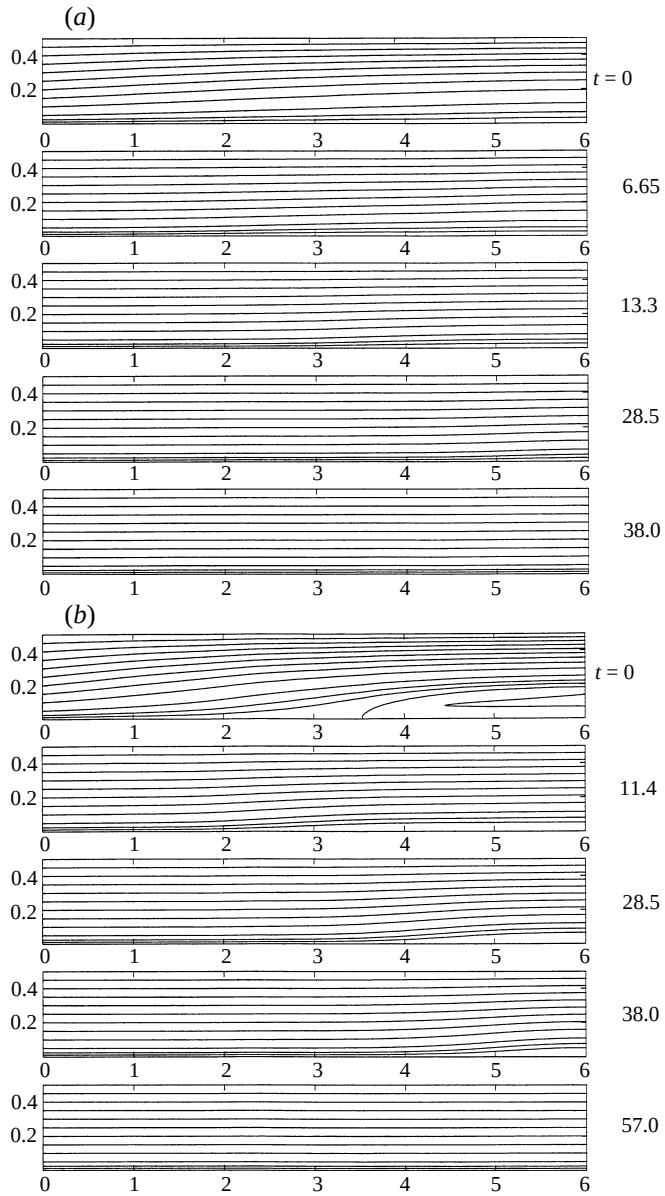

FIGURE 4. Time-history plots of stream function $\psi(x, y, t)$ for the pipe flow when $\omega = 0.7$ and (*a*) $\delta = -0.1$, (*b*) $\delta = -0.2$.

of Wang & Rusak (1996*a*) predicts, and after about 38.0 time units the flow returns to a columnar state, as expected. The convergence to a columnar state in this case is demonstrated by the time-history plots of a norm Δ_ψ^n (see again figure 5). When the perturbation becomes sufficiently small it decays exponentially with a rate of decay $\sigma \sim -0.069 w_0/r_t$.

The comparison of σ for $\omega = 0.7$ and 0.8 shows that the decay rate decreases as the swirl is increased toward the critical swirl, $\omega_1 = 0.8845$. Now, assuming that the decay rate for a small disturbance from a columnar state changes approximately as

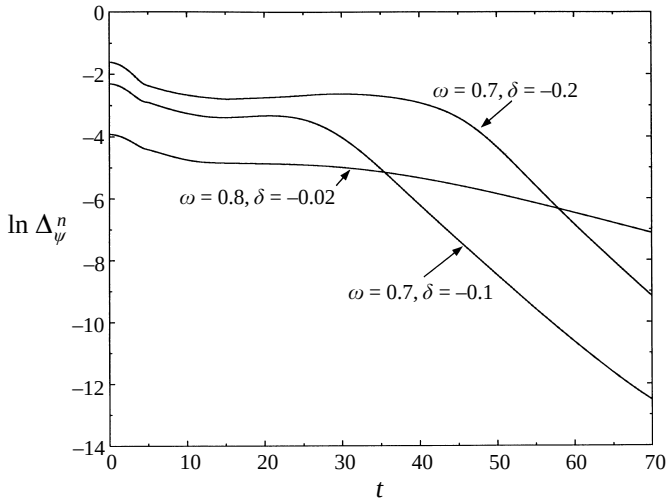

FIGURE 5. Time-history plots of the norm $\Delta_\psi^n = \max_{i,j}(|\psi_{i,j}^n - \psi_{0j}|)$ for various flow cases.

$\sigma = C_{\sigma 1}\Delta\Omega + C_{\sigma 2}(\Delta\Omega)^2 + ...$, where $\Delta\Omega = \omega^2 - \omega_1^2$, we can use the results for σ at $\omega = 0.7$ and 0.8 to find $C_{\sigma 1} \sim 0.270$ and $C_{\sigma 2} \sim -1.509$ (for a Burgers vortex with $\beta = 4.0$ and pipe length $x_0 = 6.0$). This result matches nicely with the asymptotic formula of Wang & Rusak (1996*a*, equation 50) for

$$C_{\sigma 1} = \left(\frac{\sigma}{\Delta\Omega}\right)_{\Delta\Omega \to 0} = \frac{\pi^2 w_0}{8 x_0 \omega_1^2} = 0.263$$

as well as the prediction of the loss of stability of a columnar vortex as ω approaches the critical swirl.

However, when $\delta = -0.1$ (a relatively large perturbation) we can see from the time-history plots of the functions $\psi(x, y, t)$, as well as $k(x, y, t)$ and $\chi(x, y, t)$ (figure 6*a*, *b*, *c*) that nonlinear effects become dominant and a solitary wave is created at about 57.0 time units. This solitary wave is moving upstream when $57.0 < t < 133.0$ and is then convected downstream ($133.0 < t < 209.0$) and its amplitude subsides. At about 247.0 time units a standing nonlinear wave appears, grows in size, and develops into an almost stagnant zone at about 285.0 time units. The wave of nearly stagnant flow moves upstream toward the inlet until it reaches a steady state at about 430.0 time units and stays there, as expected. It is clear that the long stagnation zone starts at a distance of about one radius from the inlet, and the flow is almost columnar after about three radii from the inlet. Also, notice the nice correlation between the states described by the stream function ψ and the circulation function k all over the time history and specifically when the stagnation zone appears and develops to steady state (figures 6*a* and 6*b*). Moreover, notice the correlation between the stream function ψ and the scaled azimuthal vorticity function, χ, near the nose of the separation zone as it develops to steady state as well as the establishment of large negative azimuthal vorticity, $\eta = (2y)^{1/2}\chi$, ahead of the stagnation point and in the surroundings of the separation line (see figures 6*a* and 6*c*). Similar behaviour of the azimuthal vorticity is also described in Lopez (1994).

This axisymmetric evolution can be observed in Sarpkaya's (1971) experiments and also in the recent experimental studies of Bruecker & Althaus (1995) and Malkiel *et al.* (1996). The growth of the axisymmetric breakdown in the experiments can be

associated with an unstable axisymmetric eigenmode disturbance near the pipe inlet and the upstream propagation of this disturbance.

The time-asymptotic state describes a transition along the pipe axis from the given inlet flow, that is significantly deflected in the radial direction, to a columnar state along most of the pipe. This state is similar to the semi-infinite open breakdown zones found by Sarpkaya (1995*a*,*b*) in swirling flows at high Reynolds numbers. The outlet states found for various pipe lengths, $x_0 = 6.0$ and 12.0, are described in figure 7 (a mesh of 400 by 30 grid points in the x- and y-directions, respectively, was used in the case where $x_0 = 12.0$). The computed outlet states are all close to the global minimizer solution of (13) with a stagnation zone as found in §3 for $\omega = 0.8$ and $\beta = 4.0$ (see figure 7). According to the theory, when x_0 is increased the outlet flow state should tend to the global minimizer solution of (13), and this is also demonstrated in figure 7.

(iii) $\omega = 1.0$: in this case $\omega > \omega_1 = 0.8845$ and the base columnar flow is unstable to axisymmetric disturbances. It is expected that the disturbances will grow and the flow may develop into a steady-state solution of a swirling flow around a stagnation zone. Starting with an initial state (18) with $\delta = -0.1$ we can see (figure 8) that the disturbance grows in time as a complicated nonlinear wave that tends to travel toward the inlet. From about 13.4 time units the wave front stays near the inlet and accumulates into a large stagnation zone that reaches a steady state after about 95.0 time units, as expected.

To demonstrate the absolute instability of the base columnar flow we also investigated the case where the initial disturbance is much smaller, $\delta = -0.02$ (see figure 9). We find that the disturbance first grows according to the linear theory (see state at time $t = 19.0$). When the disturbance is sufficiently large, nonlinear effects become evident and it is reshaped into a solitary wave near the inlet (see state at time $t = 95.0$). The wave continues to grow in time and evolves after about 437.0 time units into a steady state with a large stagnation zone that is similar to the steady state found when $\delta = -0.1$, as expected. We believe that the small differences between the steady states found for $\delta = -0.02$ and $\delta = -0.1$ should be attributed mostly to numerical inaccuracies in the time integration of the two solutions that are specifically noticeable when a line $\psi = 0.001$ (very small value) is described to represent the separation zone. It is also clear that the nose of the long stagnation zone found in the steady-state is close to the inlet and the flow is almost columnar after about two radii from the pipe inlet. Again, the steady-state solution describes a transition from the given inlet flow, that is strongly deflected in the radial direction, to a columnar state along most of the pipe that is close to the global minimizer solution of (13) with a stagnation zone as found in §3.

Again, this axisymmetric evolution can be observed in Sarpkaya's (1971) experiments and the time-asymptotic state is similar to the semi-infinite open breakdown zones found by Sarpkaya (1995*a*,*b*) in swirling flows at high Reynolds numbers and to the states found numerically by Lopez (1994).

It should be pointed out here that as δ is reduced it takes more time for the flow to evolve to the steady breakdown state. According to the stability analysis of Wang & Rusak (1996*a*) we expect that even truncation error in the numerical integration process is sufficient to excite this instability. Our experience shows that when $\omega = 1.0$ values of δ as low as -0.005 result in steady breakdown solutions; however, it takes an extremely long computation (more than 10 000 time units r_t/w_0) to derive them.

It should also be pointed out here that the theory of Wang & Rusak (1997*a*) predicts the existence of a branch of local minimizer non-columnar flow solutions when

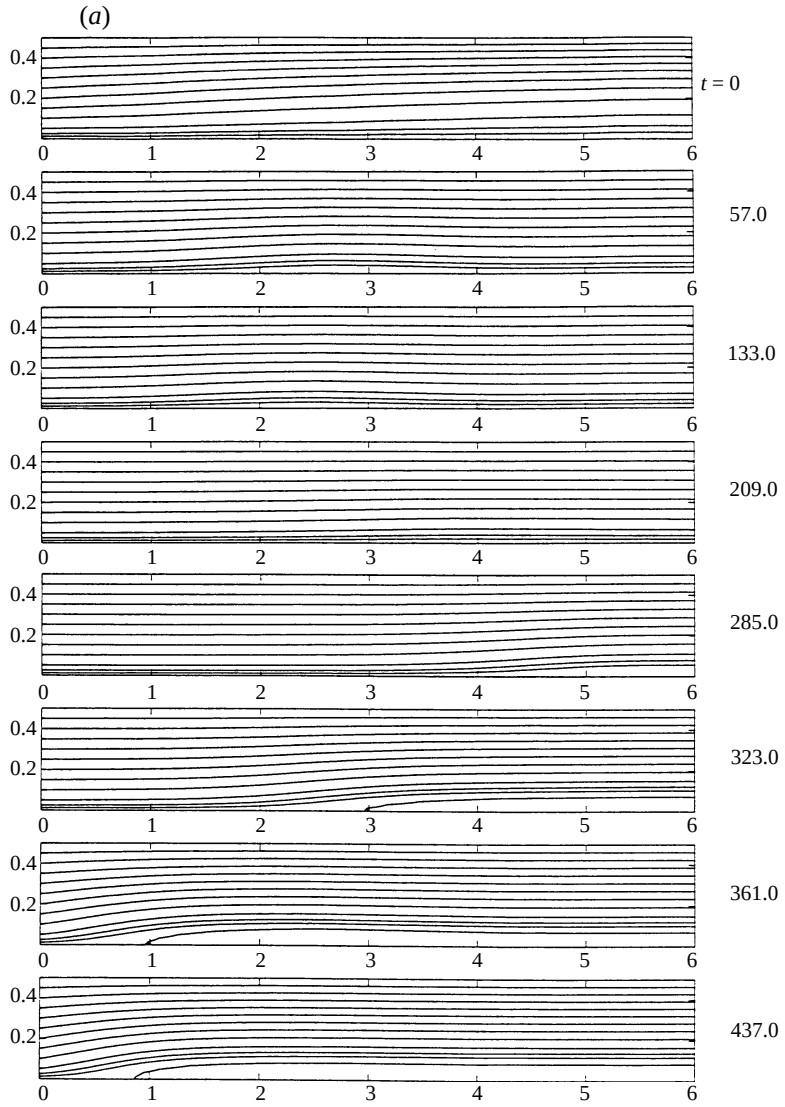

FIGURE 6(*a*). For caption see facing page.

$\omega > \omega_1$, in addition to the branch of axisymmetric breakdown states demonstrated above. This branch bifurcates at ω_1 and the solutions describe accelerating flows in the pipe with a reduced vortex core at the pipe outlet. According to the stability analysis of Wang & Rusak (1996*b*) these solutions are linearly stable but their margin of stability becomes smaller as ω approaches ω_1. Our numerical experience with the dynamics of perturbed columnar swirling flows according to (1)–(6) and (18) shows that whenever $\omega > \omega_1$ and $\delta < 0$ (the initial disturbance creates a flow deceleration) the flow always evolves into the breakdown states and we never found an evolution into the local minimizer non-columnar states. Therefore, we may conclude that these solutions are not physically realizable and the breakdown solutions dominate when $\omega > \omega_1$.

(iv) Breakdown solutions when $\omega_0 < \omega < \omega_1$: in this section we study the nature of the breakdown solutions as the swirl level of the incoming flow is reduced from

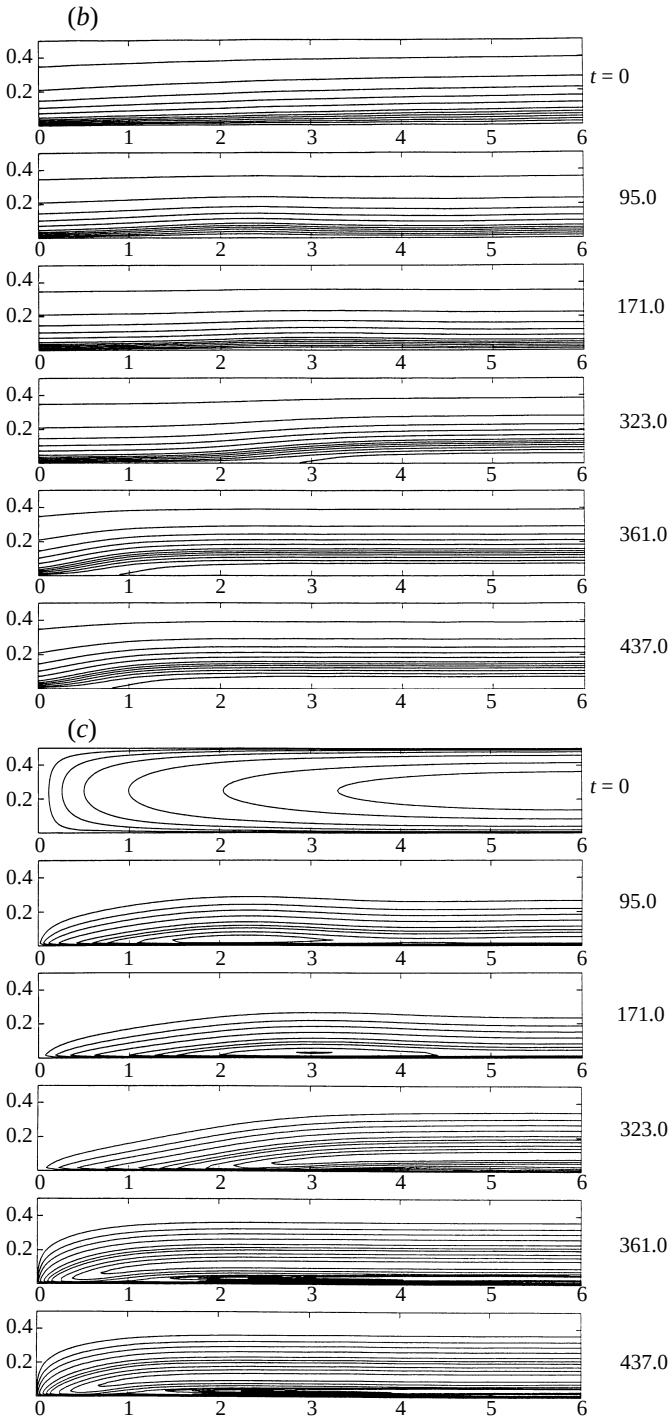

FIGURE 6. Time-history plots for the pipe flow when $\omega = 0.8$ and $\delta = -0.1$ (*a*) stream function $\psi(x, y, t)$, (*b*) circulation function $k(x, y, t)$ (lines of constant k with values $k = 0.0$, 0.005, 0.045, 0.08, 0.12, 0.16, 0.20, 0.25, 0.35, 0.45, 0.55, 0.65,0.75) and (*c*) $\chi(x, y, t)$ (lines of constant χ with values $\chi = -10.0$, -8.0, -6.0, -4.0, -3.0, -2.0, -1.0, -0.5, -0.25, -0.1, 0.0).

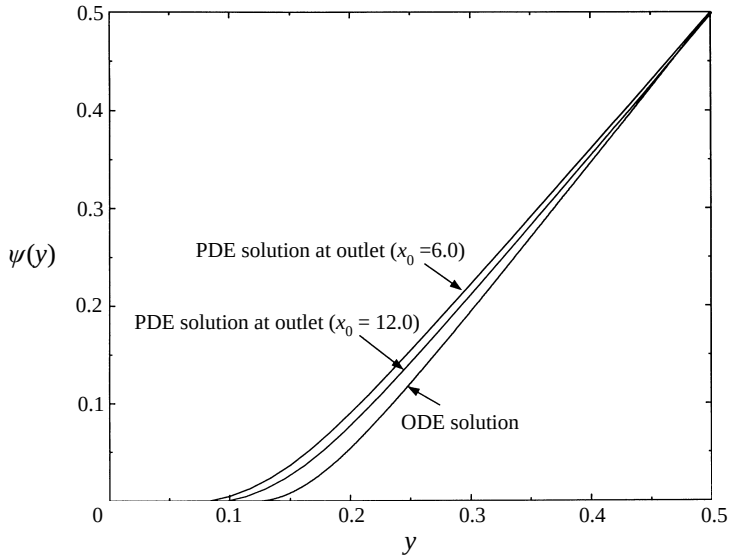

FIGURE 7. Comparison of outlet state from solution in figure 6(*a*) and the solution of (13) using a stagnation model.

$\omega = 0.8$ to $\omega_0 + \epsilon(x_0)$ (where, for $\beta = 4.0$, $\omega_0 = 0.7305$). We start from the steady breakdown solution found at $\omega = 0.8$ as an initial state, where at time $t = 0$ we reduced ω along the inlet section to 0.79. The flow develops after about 40.0 time units into the steady breakdown solution that corresponds to $\omega = 0.79$. We can see in figure 10 that this solution describes a stagnation zone that is slightly smaller than the zone in the case where $\omega = 0.8$ and its leading point is convected downstream. Using this procedure of computations, we further reduced the incoming swirl ω to 0.78 and then to 0.77 (see figure 10). We again see that the stagnation zone becomes smaller, its leading point moves downstream, and the inlet radial flow is significantly reduced as ω is reduced. This behaviour matches with the theoretical predictions of the properties of the global minimizer solution in this range of ω as discussed in Wang & Rusak (1997*a*). As we continue to reduce ω to 0.76 we find a steady-state solution after about 80.0 time units. In this case the nose of the stagnation zone moves significantly downstream to two and a half radii from the inlet and the inlet flow is very close to a columnar state (see figure 10). This indicates that the swirl level $\omega = 0.76$ is close to $\omega_0 + \epsilon(x_0)$. Further reduction of ω to 0.75 results in a motion of the stagnation zone toward the outlet. It disappears from the computational domain after about 300.0 time units and the flow returns to a steady columnar state (see figure 11). This confirms that there exists a turning point of swirl of the branch of axisymmetric breakdown solutions between 0.76 and 0.75. We now can estimate that $\epsilon(x_0) \sim 0.025$ when $x_0 = 6.0$. According to the theory, as x_0 is increased $\epsilon(x_0)$ becomes much smaller.

The process described here demonstrates that the bifurcation swirl level ω_0 is a point of exchange of stability for the branch of axisymmetric breakdown states, i.e. they are stable when $\omega > \omega_0$, become neutrally stable at $\omega = \omega_0$ and are unstable and will not exist as time-asymptotic states when $\omega < \omega_0$. Moreover, from a dynamical perspective, ω_0 is the critical level of swirl for large-amplitude axisymmetric waves in a swirling flow. When $\omega < \omega_0$ such waves may appear but over time are convected out of the flow domain. When $\omega > \omega_0$ such waves may evolve into steady breakdown zones. This special behaviour of large-amplitude disturbances and of the breakdown

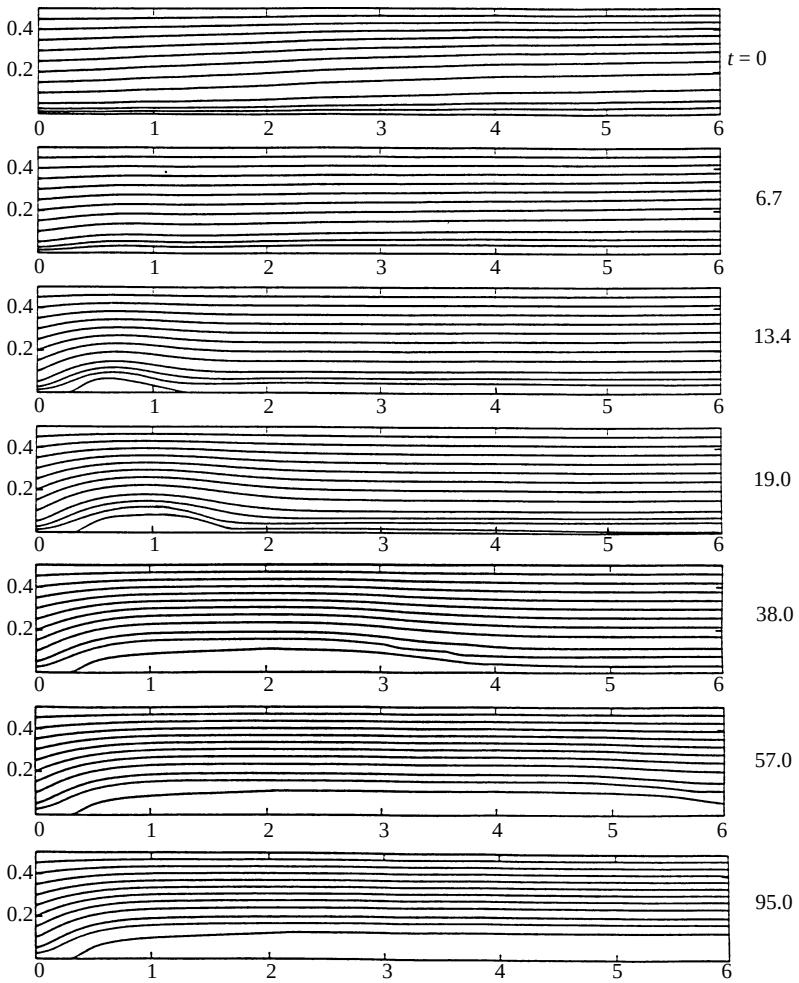

FIGURE 8. Time-history plots of stream function $\psi(x, y, t)$ for the pipe flow when $\omega = 1.0$ and $\delta = -0.1$.

states as swirl is reduced and, specifically, the loss of stability of the breakdown zone as the swirl is reduced below ω_0, is found in our experiments described in Malkiel *et al.* (1996).

5. Discussion

This paper presents numerical computations of the evolution of an inviscid, axisymmetric swirling flow in a finite-length pipe as described by the flow problem (1)–(7). These computations are the first simulations in the study of the vortex breakdown phenomenon that are guided by a consistent theory (Wang & Rusak 1997*a*). Therefore, the results obtained here can be considered reliable and help to demonstrate the predictions of the theory. We summarize the main results.

(i) The simulations demonstrate the relation between stability and criticality of columnar swirling flows and provide insight into the mechanism leading to the axisymmetric vortex breakdown phenomenon as predicted by the theory of Wang

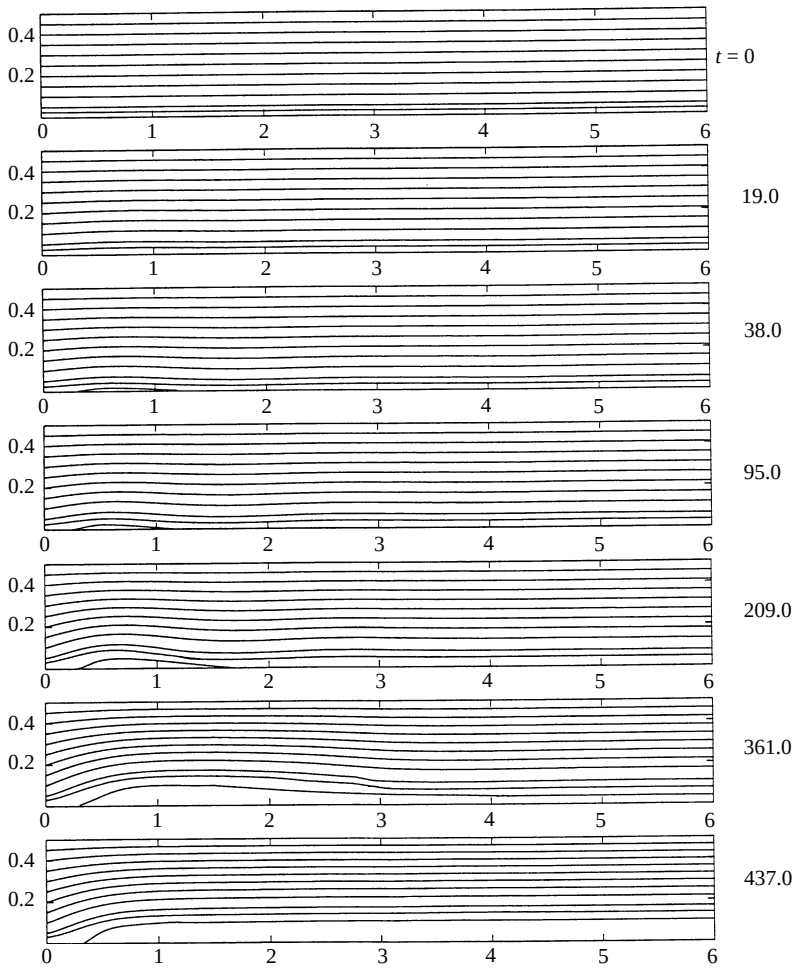

FIGURE 9. Time-history plots of stream function $\psi(x, y, t)$ for the pipe flow when $\omega = 1.0$ and $\delta = -0.02$.

& Rusak (1996*a,b*, 1997*a*). It is found that, indeed, supercritical columnar swirling flows with a swirl level less than the critical level, ω_1, are stable to small axisymmetric disturbances whereas subcritical columnar swirling flows with a swirl level greater than the critical level, ω_1, are unstable to axisymmetric disturbances. It is also interesting to notice that the rate of decay of small axisymmetric disturbances in supercritical swirling flows computed from the numerical simulations matches nicely with the asymptotic formula of Wang & Rusak (1996*a*, equation 50).

(ii) The computations shed light on the nonlinear dynamics of axisymmetric swirling flows. It is demonstrated that for the initial conditions studied in this paper, columnar swirling flows with a swirl level less than the threshold level $\omega_0 (< \omega_1)$ are unconditionally stable to any axisymmetric disturbance. In the range $\omega_0 < \omega < \omega_1$ it is demonstrated that, depending on the size of the initial disturbances, the flow may evolve into one of two distinct steady states. When the disturbances are sufficiently small they will decay in time and the flow will return to a columnar state. However, when the initial disturbances are large enough, they will grow in time and evolve nonlinearly into a large stagnation region. When $\omega > \omega_1$, it is demonstrated that the

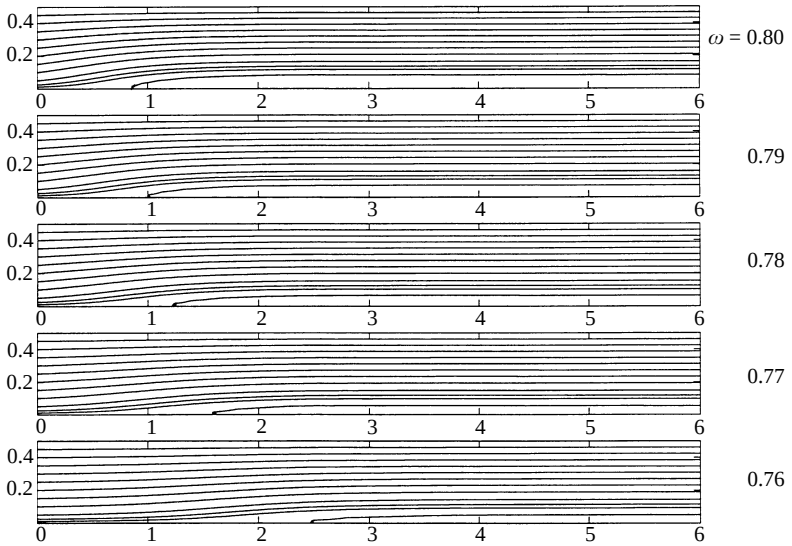

FIGURE 10. Time-asymptotic solutions of the stream function $\psi(x, y, t)$ for various levels of swirl.

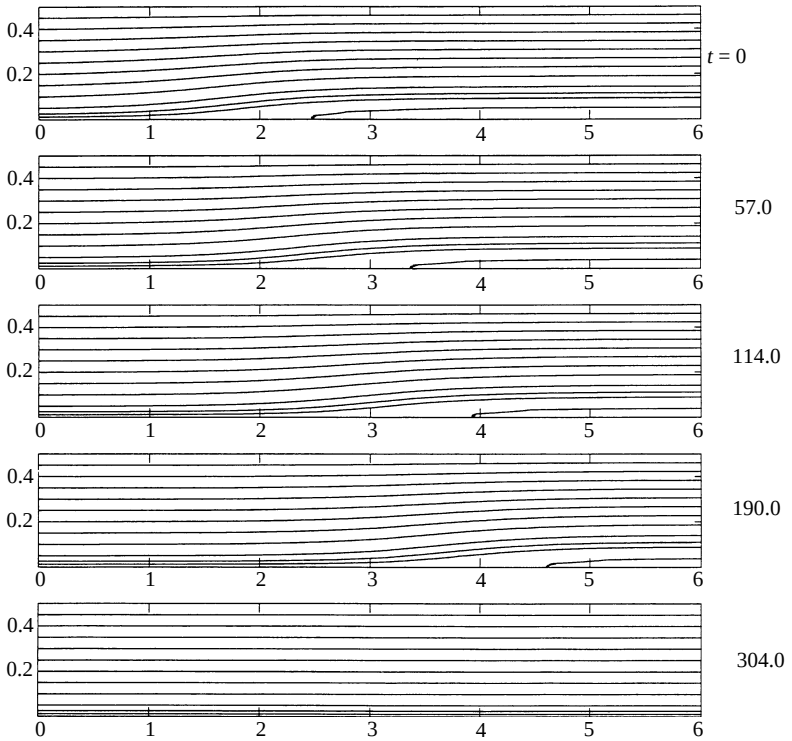

FIGURE 11. Time-history plots of stream function $\psi(x, y, t)$ for the pipe flow when ω is reduced from 0.76 to 0.75 at $t = 0$.

initial disturbances studied grow and evolve again into a vortex breakdown solution. This special behaviour of rotating flows has been predicted by our theory which the simulations serve to clarify. This dynamical behaviour is also similar to that described in the experimental studies of Sarpkaya (1971) and Malkiel *et al.* (1996).

(iii) The present inviscid and time-dependent simulations of (1)–(7) do not use any continuation model in order to establish a separation zone. Starting from the initial disturbances, the inviscid flows evolve uniquely in time and the stagnation zone naturally appears in the flow when a time-asymptotic state is reached. As a result, the computations provide strong evidence that, within the inviscid and steady-state framework, while looking for solutions of the Squire–Long equation, the stagnation model is the relevant model to be used to describe a separation zone. Therefore, the computation of breakdown solutions of the SLE (8) with boundary conditions (9) should use this methodology. Such behaviour is also consistent with the results of viscous numerical simulations in high-Reynolds-number flows, experimental data about the flow nature inside the breakdown zones and matches the expected behaviour of viscous axisymmetric separation zones in the inviscid limit case.

(iv) We have shown in our analysis of solutions of the SLE(8), (9), that there exists a threshold value of swirl, ω_0, where breakdown solutions can be found only when $\omega > \omega_0$ and where these solutions are global minimizer solutions of the equation. We have also shown that these solutions are strongly related to global minimizer solutions of the ODE (11) resulting from the SLE and that the value of ω_0 is found when the global minimizer solution of the columnar problem is no longer the base flow. However, in this ODE framework the value of ω_0 depends on the choice of a continuation model. The present computations clarify that using the stagnation model in the search for solutions of the columnar problem (11) is indeed the relevant way of computing ω_0 as has been suggested by Wang & Rusak (1997*a*).

(v) The present simulations construct the global minimizer solutions of the SLE (8), (9) when $\omega > \omega_0 + \epsilon(x_0)$ from the dynamical process given by (1)–(7). This branch describes breakdown solutions which are stable to axisymmetric disturbances for any $\omega > \omega_0 + \epsilon(x_0)$. However, as the inlet swirl is decreased toward $\omega_0 + \epsilon(x_0)$ the solutions describe a stagnation zone whose nose tends to move downstream toward the pipe outlet and the margin of stability of those solutions becomes smaller. When $\omega < \omega_0 + \epsilon(x_0)$, no standing wave can be sustained in the flow and the branch of breakdown solutions ceases to exist. It should also be pointed out that our computations show that the branch of min-max solutions of the SLE (8), (9) in the range $\omega_0 + \epsilon(x_0) < \omega < \omega_1$, that connects the branch of columnar solutions with the branch of breakdown solutions, cannot be accessed from the dynamical process described by (1)–(7). This result matches with the theoretical predictions of Wang & Rusak (1996*b*) that these solutions are unstable to axisymmetric disturbances.

(vi) It should be pointed out that the numerical simulations of Lopez (1994) using the axisymmetric, time-dependent Navier–Stokes equations, also show that for sufficiently high Reynolds numbers, the separation zones in breakdown solutions become longer and essentially regions of stagnant flow as Reynolds number is increased. These zones are similar in nature to those found in our inviscid computations. Moreover, the size of the separation zones in the viscous computations of Lopez (1994) is comparable to that predicted by our analysis using solutions of the ODE (11). Lopez (1994) also suggested that viscous dissipation is responsible for closing the separation zone, not the downstream boundary condition. This suggests that in the inviscid limit of viscous calculations the axisymmetric breakdown zone will become longer and an open separation zone will appear, as predicted in our inviscid theory

of Wang & Rusak (1997*a*). Furthermore, Lopez (1994) showed that the level of swirl above which breakdown solutions can be found (his secondary limit point) for an inlet Burgers vortex with $\beta = 4.0$ tends to a certain value $V = 1.466$ as the Reynolds number is increased. Using our method of computing ω_0 we find that the threshold value for the appearance of inviscid breakdown solutions for a very long pipe, in the scale of Lopez's (1994) or Beran & Culick's (1992) computations $V = 2\omega$, is 1.461 which is in very good agreement with the viscous computations. This demonstrates the nature of the swirl level, ω_0 (of Keller *et al.* 1985), as a critical swirl related to the secondary limit point found in the Navier–Stokes computations of Beran & Culick (1992), Beran (1994) and Lopez (1994).

(vii) The details of the computations described in figures 4–11 provide insight into the dynamics of both small- and large-amplitude waves in a swirling flow. When the disturbances are sufficiently small, the linear theory may apply and base columnar flows can be classified as supercritical when $\omega < \omega_1$ and subcritical when $\omega > \omega_1$. Supercritical swirling flows can sustain only small-amplitude waves that travel downstream. On the other hand, subcritical swirling flows allow small-amplitude waves to travel upstream and due to the interaction with the inlet flow state they become unstable and grow. When large-amplitude disturbances are imposed on the flow at the initial state, the behaviour is more complicated and is related with the nonlinear effects. Supercritical swirling flows with $\omega < \omega_0$ can sustain only large-amplitude waves that travel downstream. However, when $\omega > \omega_0$, the swirling flow allows large-amplitude waves to travel upstream and create a large standing wave with a stagnation zone. From this dynamical perspective, ω_0 is the critical level of swirl for large-amplitude axisymmetric disturbances in a swirling flow. The dynamical behaviour of small- and large-amplitude disturbances described here matches nicely with available experimental data.

(viii) We also want to point out that nonlinear effects tend to reshape the initial disturbances after some time into solitary waves that travel in the flow and we may find for a certain time period flow states that are close to the states described by the min-max solutions. However, those states continue to develop in time and either travel downstream and out of the flow domain (see figures 4*a*, 4*b*), or evolve into a large amplitude standing wave with a stagnation zone (see figures 6, 8 and 9). The certain transient states where small-amplitude solitary travelling waves appear in the flow may be described by a weakly nonlinear analysis similar to the theory of Randall & Leibovich (1973).

It can be concluded that the axisymmetric vortex breakdown process in high-Reynolds-number flows in a straight pipe is the evolution, that occurs only when $\omega > \omega_0$, from a columnar vortex flow, that loses its stability when ω is near or above ω_1, into another steady and stable (supercritical) global minimizer state that is a strong attractor. This inviscid equilibrium state describes an almost stagnant zone in the flow. This state is a spatial transition from a given swirling flow along the inlet, that is deflected in the radial direction, to a columnar (supercritical) state described by the global minimizer solution of the columnar Squire–Long equation when $\omega > \omega_0$. When $\omega_0 < \omega < \omega_1$ only finite perturbations of the order of $\omega_1 - \omega$ will induce this transition process, whereas when $\omega > \omega_1$, any perturbation will induce this transition. Figure 3 provides the guiding criteria for the appearance of axisymmetric vortex breakdown in a Burgers vortex coming into a pipe and figure 1 provides the downstream columnar state of the inviscid breakdown solution and the characteristic size of the breakdown zone. The information in figures 1 and 3 can be used in any future computations of vortex breakdown in Burgers vortex flows in a pipe. The

method described in this paper can be used to calculate similar criteria for any swirling flow of engineering interest. For example, such recent calculations of the breakdown characteristics of a Q-vortex in a pipe and their correlation to experimental data are reported in Rusak, Whiting & Wang (1997). The present paper also demonstrates the relation between several previous approaches to explain the vortex breakdown phenomenon. It connects between the recent results on hydrodynamic stability (Wang & Rusak 1996*a,b*), the critical state theory of Benjamin (1962), the bifurcation analysis of Leibovich & Kribus (1990), the stagnation zones approach of Keller *et al.* (1985) and the Navier–Stokes solutions of Beran & Culick (1992), Beran (1994) and Lopez (1994).

This research was carried out with the support of the National Science Foundation under Grant CTS-9310181. Partial support was also given by the U.S. – Israel Binational Science Foundation under Grant 94-00245/1.

REFERENCES

Althaus, W., Bruecker, Ch. & Weimer, M. 1995 Breakdown of slender vortices. In *Fluid Vortices* (ed. S. I. Green), pp. 373–426. Kluwer.

Ash, R. L. & Khorrami, M. R. 1995 Vortex stability. In *Fluid Vortices* (ed. S. I. Green), pp. 317–372. Kluwer.

Batchelor, G. K. 1967 *An Introduction to Fluid Dynamics*. Cambridge University Press.

Benjamin, T. B. 1962 Theory of the vortex breakdown phenomenon. *J. Fluid Mech.* **14**, 593–629.

Beran, P. S. 1994 The time-asymptotic behaviour of vortex breakdown in tubes'. *Computers Fluids* **23**, 913–937.

Beran, P. S. & Culick, F. E. C. 1992 The role of non-uniqueness in the development of vortex breakdown in tubes. *J. Fluid Mech.* **242**, 491–527.

Bragg, S. L. & Hawthorne, W. R. 1950 Some exact solutions of the flow through annular cascade actuator discs. *J. Aero. Sci.* **17**, 243–249.

Bruecker, Ch. & Althaus, W. 1995 Study of vortex breakdown by particle tracking velocimetry (PTV), Part 3: Time-dependent structure and development of breakdown modes. *Exps. Fluids* **18**, 174–186.

Buntine, J. D. & Saffman, P. G. 1995 Inviscid swirling flows and vortex breakdown. *Proc. R. Soc. Lond.* A **449**, 139–153.

Cary, A. W., Darmofal, D. L. & Powell, K. G. 1997 Onset of the spiral mode of vortex breakdown. *AIAA Paper* 97-0439.

Delery, J. M. 1994 Aspects of vortex breakdown. *Prog. Aerospace Sci.* **30**, 1.

Drazin, P. G. & Howard, L. N. 1966 Hydrodynamic stability of parallel flow of inviscid fluid. *Adv. Appl. Mech.* **9**, 1–90.

Escudier, M. 1988 Vortex breakdown: observations and explanations. *Prog. Aerospace Sci.* **25**, 189–229.

Grabowski, W. J. & Berger, S. A. 1976 Solutions of the Navier–Stokes equations for vortex breakdown. *J. Fluid Mech.* **73**, 525–544.

Hafez, M. M. & Salas, M. D. 1985 Vortex breakdown simulation based on nonlinear inviscid model. In *Studies of Vortex Dominated Flows* (ed. M. Y. Hussaini & M. D. Salas), pp. 76–83. Springer.

Hall, M. G. 1972 Vortex breakdown. *Ann. Rev. Fluid Mech.* **4**, 195–217.

Keller, J. J., Egli, W., & Exley, W. 1985 Force- and loss-free transitions between flow states. *Z. Angew. Math. Phys.* **36**, 854–889.

Kopecky, R. M. & Torrance, K. E. 1973 Initiation and structure of axisymmetric. *Comput. Fluids* **1**, 289–300.

Krause, E. 1985 Pressure variation in axially symmetric breakdown. *Proc. Colloq. on Vortex Breakdown, Feb. 11-12, RWTH Aachen*, pp. 49–68.

Leibovich, S. 1978 The structure of vortex breakdown. *Ann. Rev. Fluid Mech.* **10**, 221–246.

Leibovich, S. 1984 Vortex stability and breakdown: survey and extension. *AIAA J.* **22**, 1192–1206.

Leibovich, S. & Kribus, A. 1990 Large amplitude wavetrains and solitary waves in vortices. *J. Fluid Mech.* **216**, 459–504.

Lopez, J. M. 1994 On the bifurcation structure of axisymmetric vortex breakdown in a constricted pipe. *Phys. Fluids* **6**, 3683–3693.

Malkiel, E., Cohen, J., Rusak, Z. & Wang, S. 1996 Axisymmetric vortex breakdown in a pipe-theoretical and experimental studies. *Proc. 36th Israel Annual Conf. on Aerospace Sciences* (*February*), pp. 24–34.

Menne, S. 1988 Simulations of vortex breakdown in tubes. *AIAA Paper* 88-3575.

Randall, J. D. & Leibovich, S. 1973 The critical state: a trapped wave model of vortex breakdown. *J. Fluid Mech.* **53**, 481–493.

Rusak, Z., Judd, K. P. & Wang, S. 1997 The effect of small pipe divergence on near critical swirling flows. *Phys. Fluids* **9**, 2273–2285.

Rusak, Z. & Wang, S. 1996*a* Review of theoretical approaches to the vortex breakdown phenomenon. *AIAA Paper* 96-2126.

Rusak, Z. & Wang, S. 1996*b* Theoretical study of the axisymmetric vortex breakdown phenomenon. In *Proc. Applied Mathematics 84: Mathematics is for Solving Problems; A volume in honor of Julian Cole's 70th Birthday* (ed. P. L. Cook, V. Roytburd & M. Tulin). SIAM.

Rusak, Z., Whiting, C. H. & Wang, S. 1997 Axisymmetric breakdown of a Q-vortex in a pipe. *AIAA Paper* 97-0441.

Salas, M. D. & Kuruvila, G. 1989 Vortex breakdown simulation: a circumspect study of the steady, laminar, axisymmetric model. *Computers Fluids* **17**, 247–262.

Sarpkaya T. 1971 On stationary and traveling vortex breakdowns. *J. Fluid Mech.* **45**, 545–559.

Sarpkaya, T. 1995*a* Vortex breakdown and turbulence. *AIAA Paper* 95-0433.

Sarpkaya, T. 1995*b* Turbulent vortex breakdown. *Phys. Fluids* **7**, 2301–2303.

Spall, R. E. 1996 Transition from spiral- to bubble-type vortex breakdown. *Phys. Fluids* **8**, 1330–1332.

Spall, R. E. & Gatski, T. B. 1991 A computational study of the topology of vortex breakdown. *Proc. R. Soc. Lond.* A **435**, 321–337.

Szeri, A. & Holmes, P. 1988 Nonlinear stability of axisymmetric swirling flows. *Phil. Trans. R. Soc. Lond.* A **326**, 327–354.

Tromp, J. C. & Beran, P. S. 1996 Temporal evolution of three-dimensional vortex breakdown from steady, axisymmetric solutions. *AIAA J.* **34**, 632–634.

Tromp, J. C. & Beran, P. S. 1997 The role of nonunique axisymmetric solutions in 3-D vortex breakdown. *Phys. Fluids* **9**, 992–1002.

Visbal, M. R. 1996 Computed unsteady structure of spiral vortex breakdown on delta wings. *AIAA Paper* 96-2074.

Wang, S. & Rusak, Z. 1996*a* On the stability of an axisymmetric rotating flow in a pipe. *Phys. Fluids* **8**, 1007–1016.

Wang, S. & Rusak, Z. 1996*b* On the stability of non-columnar swirling flows. *Phys. Fluids* **8**, 1017–1023.

Wang, S. & Rusak, Z. 1996*c* Axisymmetric vortex breakdown in a pipe. *ESAIM (European Series in Applied and Industrial Mathematics) Proc.*, **1**, 267–278 (electronic journal address: http://www.emath.fr/proc/Vol.1/).

Wang, S. & Rusak, Z. 1997*a* The dynamics of a swirling flow in a pipe and transition to axisymmetric vortex breakdown. *J. Fluid Mech.* **340**, 177–223.

Wang, S. & Rusak, Z. 1997*b* The effect of slight viscosity on near critical swirling flows. *Phys. Fluids* **9**, 1914–1927.

Whiting, C. H. 1996 Analysis of the vortex breakdown phenomenon. MSc Thesis, Rensselaer Polytechnic Institute, Troy, NY.